JUDD-OFELT ANALYSIS AND CONCENTRATION-DEPENDENT LUMINESCENCE QUENCHING BEHAVIOR OF DY³⁺-DOPED NAYGEO₄ Phosphors Prepared by Solid-State Reaction

SHENGYI LIU 1,* , DUAN GAO 2 , JIADE DONG 1 , HAN YIN 1 , HAOYU LIU 1 , LI WANG 1 , WENBIN SONG 1

- ¹ School of Intelligence and Electronic Engineering, Dalian Neusoft University of Information, Dalian, Liaoning 116026, China
- ² Department of Public Security Management, Liaoning Police College, Dalian, Liaoning 116036, China
- *Corresponding author: liushengyi@neusoft.edu.cn

Received: 21.10.2025

Abstract. In this study, a series of NaYGeO₄ (NYG): Dy³⁺ phosphors with varying Dy³⁺ doping concentrations were successfully synthesized via a conventional high-temperature solid-state reaction method. X-ray diffraction analysis confirmed that all samples exhibited a pure NYG phase with no detectable secondary phases. To systematically investigate the concentration quenching behavior and thermal stability of luminescence, the photoluminescence properties of the samples were comprehensively characterized. In addition, diffuse reflectance spectra, fluorescence decay measurements, and Judd-Ofelt theory were employed to gain deeper insight into the optical transition characteristics of Dy³⁺ ions. The results indicate that the internal quantum efficiency of the Dy³⁺ 4 F9/ 2 level gradually decreases with increasing dopant concentration.

Keywords: luminescence, Judd-Ofelt theory, NaYGeO4, phosphors

UDC: 535.37

DOI: 10.3116/16091833/Ukr.J.Phys.Opt.2026.01040

This work is licensed under the Creative Commons Attribution International License (CC BY 4.0).

1. Introduction

Rare-earth ion-doped materials have long attracted considerable attention due to their widespread applications in lighting and laser sources, display devices, biomedicine, optical detection, and sensing technologies[1-5]. Dy³+, another important trivalent rare-earth ion, is capable of simultaneously producing blue and yellow emissions corresponding to the ${}^4F_{9/2} \rightarrow {}^6H_{15/2}$ and ${}^4F_{9/2} \rightarrow {}^6H_{13/2}$ transitions, respectively [6-8]. The former is a typical electric dipole transition with a relatively weak dependence on the host lattice. In contrast, the latter is a hypersensitive transition that shows a strong dependence on the local crystal-field environment. This differential sensitivity allows the relative intensity ratio between the yellow and blue emissions to be finely tuned by modifying or selecting suitable host lattices, thereby enabling white light generation. Consequently, Dy³+-doped materials have been recognized as promising candidates for white LED applications and warrant further investigation [9,10].

In recent years, germanate compounds have emerged as attractive host matrices for phosphor design due to their relatively low synthesis temperatures and excellent physical and chemical stability. Germanate-based phosphors typically exhibit outstanding thermal stability and excellent luminescent properties, showing great potential for applications in lighting, displays, biomedical imaging, and solar cells. Although previous studies have investigated the luminescence properties of NaYGeO $_4$ -based systems – such as NaYGeO $_4$:Eu $_4$ -/Sm $_4$ -/Dy $_4$ -based systems – such as NaYGeO $_4$:Eu $_4$ -/Sm $_4$ -/Dy $_4$ -based systems – such as NaYGeO $_4$:Eu $_4$ -/Sm $_4$ -/Dy $_4$ -based systems – such as NaYGeO $_4$:Eu $_4$ -/Sm $_4$

Jie Zhang et al. [11] and NaYGeO₄: Bi³⁺/Tb³⁺/Eu³⁺ by Erlei Wang et al.[12], as well as the anticounterfeiting potential of NaYGeO₄: Tb³⁺ reported by Wenyu Zhao et al.[13] – systematic studies focusing on the optical transition characteristics of singly Dy³⁺-doped NaYGeO₄ phosphors remain scarce. Moreover, their application in temperature sensing has yet to be explored. Therefore, developing Dy³⁺-doped NaYGeO₄ phosphors may open new possibilities for industrial and optical applications.

In this study, a series of NaYGeO₄: x Dy³⁺ (NYG: x Dy³⁺) phosphors was successfully synthesized. The NYG host not only provides suitable lattice sites for Dy³⁺ incorporation but also possesses a wide band gap of 5.493-5.864 eV. The effects of Dy³⁺ doping concentration on luminescence intensity, quantum efficiency, and optical transition characteristics were systematically investigated. Furthermore, the Judd-Ofelt parameters of NYG: Dy³⁺ at various doping concentrations were calculated from diffuse reflectance spectra, providing deeper insights into the optical transition behavior of Dy³⁺ ions. The results indicate that NYG: Dy³⁺ phosphors exhibit promising potential for applications in white LEDs and optical temperature sensors.

2.2. Experimental section

2.1. Raw materials preparation

The raw materials used in this study were sodium carbonate (Na₂CO₃, 99.9%), yttrium oxide (Y₂O₃, 99.99%), germanium dioxide (GeO₂, 99.8%), and dysprosium oxide (Dy₂O₃, 99.99%), all purchased from Tianjin Jinke Fine Chemical Research Institute. These analytical-grade reagents were used as received without further purification. The synthesis process was as follows: First, stoichiometric amounts of raw materials corresponding to the target Dy³⁺ concentration were precisely weighed using an electronic balance and mixed thoroughly in an agate mortar with ethanol as a dispersant for 30 min to ensure homogeneity. The resulting slurry was dried in the oven, ground to a fine powder, and then transferred to alumina crucibles. The mixtures were placed in a high-temperature furnace and heated from room temperature (~20 °C) to 1200 °C at approximately 10 °C/min, then maintained at 1200 °C for 4 h for calcination. Afterward, the samples were allowed to cool naturally to room temperature inside the furnace.

2.2. Characterization

The phase composition of the samples was characterized using a Shimadzu XRD-6000 powder X-ray diffractometer with Cu K α_1 radiation (λ = 0.15406 nm). The diffraction patterns were recorded in the 20 range of 10°-80° with a step size of 0.02°. Fluorescence decay curves were measured using an Edinburgh Instruments FLS1000 fluorescence spectrometer, equipped with a powder sample holder. Diffuse reflectance spectra (DRS) were obtained using a Shimadzu UV-3600 UV-Vis-NIR spectrophotometer fitted with an integrating sphere accessory (Model 206-23851-91, provided by Antai Co., China).

3. Results and discussion

3.1. Crystal structure

To verify the successful synthesis of NYG: x Dy³⁺ phosphors, both the crystal structure and microstructure were systematically analyzed. Structural analysis revealed that NYG crystallizes in an orthorhombic system with space group Pnma (No. 62). The refined lattice parameters are a = 11.28 Å, b = 6.42 Å, c = 5.17 Å, $\alpha = \beta = \gamma = 90^{\circ}$, and a unit cell volume $V = 374.39899 \text{ Å}^3$. The

NYG structure consists of three cationic polyhedral – [GeO₄] tetrahedra, [NaO₆], and [YO₆] octahedra–which are interconnected via corner- and edge-sharing (Fig. 1a). Because Dy³⁺ (r = 0.912 Å, CN = 6) and Y³⁺ (r = 1.040 Å, CN = 6) possess similar valence states, coordination numbers, and ionic radii, Dy³⁺ ions can easily substitute for Y³⁺ sites in the NYG lattice, enabling effective incorporation and luminescence. The XRD pattern of the representative NYG: 4 mol% Dy³⁺ sample matches well with the standard pattern of the NYG host (JCPDS #88-1177), confirming phase purity (Fig. 1c). Fig. 1b display the diffuse reflectance (DR) spectra of NYG: 4 mol% Dy³⁺ samples. A pronounced high-reflectance region is observed in the range of approximately 500-700 nm, while a significant decrease in reflectance occurs in the 200-250 nm region. The optical band gap (E_{opt}) of NYG can be estimated using the Kubelka-Munk function combined with the Tauc plot method. When the incident photon energy (hv) satisfies $hv \ge E_{opt}$, electrons can be excited from the valence band to the conduction band through intrinsic transitions. The quantitative relationship is expressed by Eq. (1-2) [14-15]:

$$F(R) = \frac{(1-R)^n}{2R} \quad , \tag{1}$$

$$[F(R)hv]^{2} = A(hv - E_{g}).$$
 (2)

Here, F(R) represents the Kubelka-Munk function, R denotes the reflectance (%), n = 1/2 corresponds to the indirect band gap, A is a proportionality constant related to the intrinsic properties of the material, h is Planck's constant ($h \approx 6.626 \times 10^{-34} \, \text{J} \times \text{s}$), ν is the frequency of the incident light, $h\nu$ represents the photon energy, and E_g denotes the optical band gap energy.

According to the relation ($[F(R)hv]^2 = 0$), a tangent line is drawn near the linear region of the curve (with the maximum slope). The intersection point of this tangent with the horizontal axis ($[F(R)hv]^2 = 0$) corresponds to the optical band gap ($E_{\rm opt}$). The obtained $E_{\rm opt}$ values are 5.511 eV ($x = 1 \, {\rm mol}\%$), 5.493 eV ($x = 2 \, {\rm mol}\%$), 5.859 eV ($x = 4 \, {\rm mol}\%$), 5.864 eV ($x = 6 \, {\rm mol}\%$), 5.723 eV ($x = 8 \, {\rm mol}\%$), and 5.561 eV ($x = 10 \, {\rm mol}\%$), respectively.

These results indicate that the NYG host possesses a wide band gap, confirming its suitability as an efficient luminescent matrix that can accommodate both ground and excited states of activator ions. The band gap of NYG: x Dy $^{3+}$ exhibits a slight dependence on the Dy $^{3+}$ doping concentration, which can be attributed to the influence of Dy $^{3+}$ 4f energy levels on the host's electronic band structure. Furthermore, to facilitate the subsequent calculation of Judd-Ofelt (J–O) intensity parameters, the empirical Herve-Vandamme relation (Eq. (3)) was employed to estimate the refractive index (n) of the samples[16-18].

$$n = \sqrt{1 + \left(\frac{A}{E_{opt} + B}\right)^2} \quad . \tag{3}$$

Here, n denotes the refractive index of the sample; the empirical constants are $A=13.6\,\mathrm{eV}$ and $B=3.4\,\mathrm{eV}$. By substituting the previously determined optical band gap values into the calculation, the refractive indices of NYG: x Dy³+ phosphors were obtained as 1.825 ($x=1\,\mathrm{mol\%}$), 1.827 ($x=2\,\mathrm{mol\%}$), 1.777 ($x=4\,\mathrm{mol\%}$), 1.776 ($x=6\,\mathrm{mol\%}$), 1.795 ($x=8\,\mathrm{mol\%}$), and 1.818 ($x=10\,\mathrm{mol\%}$). The refractive index similarly exhibits a slight dependence on the Dy³+ doping concentration. These values serve as essential optical parameters, particularly the refractive index of the lowest-doped sample, $n(x=1\,\mathrm{mol\%})=1.825$, which will be used in Section 3.3 to calculate J-O intensity parameters.

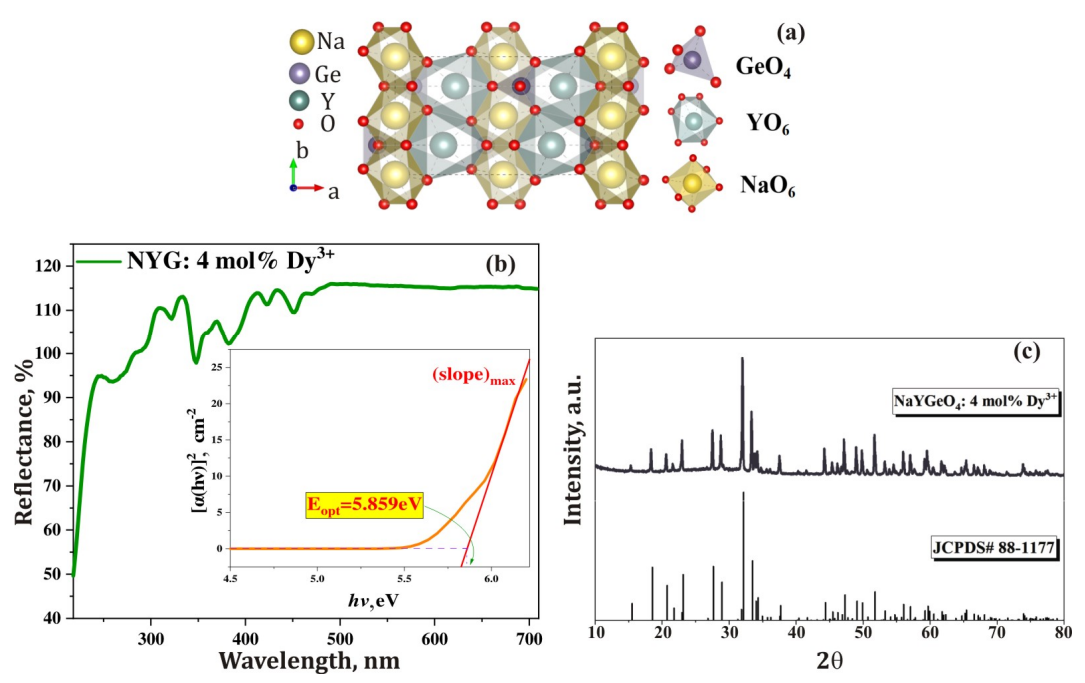


Fig. 1. (a) Crystal structure of NYG; (b) Diffuse reflectance spectrum of NYG: 4 mol% Dy³⁺, inset shows the optical band gap calculation; (c) XRD pattern of a representative NYG: 4 mol% Dy³⁺ sample and the standard diffraction pattern of NYG (JCPDS#88-1177).

3.2. Photoluminescence properties

After establishing the crystal field characteristics of the NYG host, this study further focused on the photoluminescence (PL) properties of a series of NYG: x Dy³+ (x = 1, 2, 4, 6, 8, 10 mol%) samples. As shown in Fig. 2a, the photoluminescence excitation (PLE) spectra were recorded by monitoring the characteristic ${}^4F_{9/2} \rightarrow {}^6H_{13/2}$ emission of Dy³+ at 578 nm. The PLE spectra, measured in the 200-500 nm range, can be divided into two main regions. The broad excitation band from 200 to 282 nm is attributed to the charge transfer band (CTB) from O^2 - to Dy³+ In contrast, the eight sharp narrow peaks observed between ~282 and 500 nm correspond to the intra-4f forbidden transitions of the Dy³+ emission center, namely: ${}^6H_{15/2} \rightarrow {}^4D_{7/2}$ (294 nm), ${}^6H_{15/2} \rightarrow {}^6P_{3/2}$ (322 nm), ${}^6H_{15/2} \rightarrow {}^6P_{7/2}$ (346 nm), ${}^6H_{15/2} \rightarrow {}^6P_{5/2}$ (364 nm), ${}^6H_{15/2} \rightarrow {}^4I_{13/2}$ (382 nm), ${}^6H_{15/2} \rightarrow {}^4G_{11/2}$ (424 nm), ${}^6H_{15/2} \rightarrow {}^4I_{15/2}$ (452 nm), and ${}^6H_{15/2} \rightarrow {}^4F_{9/2}$ (472 nm). Notably, the most intense excitation peak at 346 nm initially increases with Dy³+ concentration and then decreases, as shown in Fig. 2b.

The PL spectra of NYG: x Dy³+ under 346 nm excitation are presented in Fig. 2c. Three main sharp emission peaks are observed: ${}^4F_{9/2} \rightarrow {}^6H_{15/2}$ (486 nm, blue), ${}^4F_{9/2} \rightarrow {}^6H_{13/2}$ (578 nm, yellow), and ${}^4F_{9/2} \rightarrow {}^6H_{11/2}$ (660 nm, red). The 486 nm emission corresponds to a magnetic dipole (MD) transition and is almost insensitive to the surrounding crystal field. Conversely, the 578 nm emission is highly sensitive to the local symmetry of Dy³+ ions in the NYG host, as it arises from a pure electric dipole (ED) transition. Since the intensity of ED transitions is stronger than that of MD transitions, it is inferred that Dy³+ ions occupy the low-symmetry Y³+ sites in NYG. In the crystal structure of NYG, Na³+/Y³+ ions are coordinated with six oxygen atoms to form [NaO₆] and [YO₆] octahedra, with Na/Y-O distances of 2.245, 2.197, 2.245, and 2.488 Å, respectively. The sharp emission peaks in the PL spectra correspond well to the energy level diagram of Dy³+

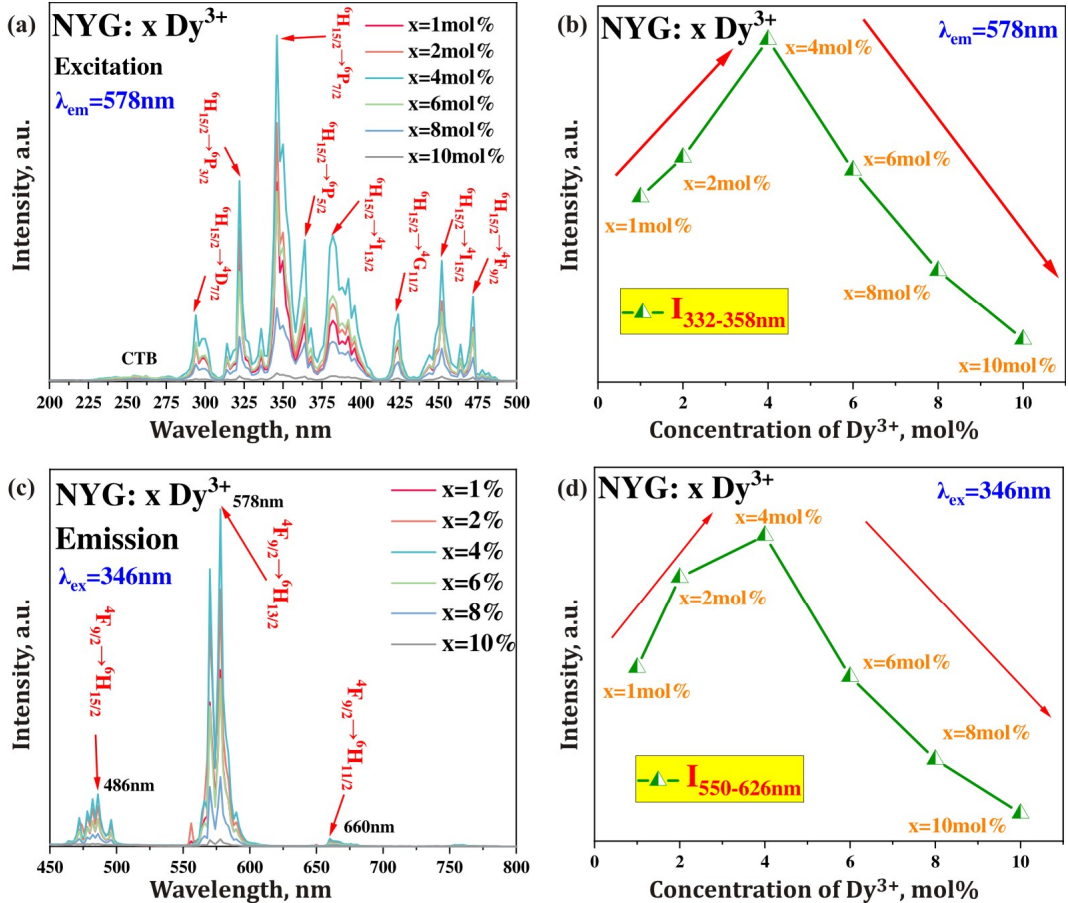


Fig. 2. (a) PLE spectra of NYG: x Dy³⁺ samples; (b) Plot of the integrated excitation peak intensity in the 332-358 nm range versus Dy³⁺ doping concentration; (c) PL spectra of NYG: x Dy³⁺ samples; (d) Plot of the integrated emission peak intensity in the 550-626 nm range versus Dy³⁺ doping concentration.

shown in Fig. 3. Under 346 nm excitation, electrons are promoted from the ground state $^6H_{15/2}$ to the higher $^6P_{7/2}$ level and then relax non-radiatively (NR) to the $^4F_{9/2}$ state. Finally, radiative transitions from $^4F_{9/2}$ to $^6H_{J/2}$ (J = 15, 13, 11) yield the observed 486 nm (blue), 578 nm (yellow), and 660 nm (red) emissions.

The $^4F_{9/2} \rightarrow ^6H_{15/2}$ (486 nm) and $^4F_{9/2} \rightarrow ^6H_{13/2}$ (578 nm) emissions correspond to the MD and hypersensitive ED transitions of Dy³+, respectively. While the MD transition is nearly unaffected by the crystal field, the ED transition is highly sensitive to the local symmetry around Dy³+ in the host lattice. The yellow emission at 578 nm, a hypersensitive transition ($\Delta L = 2$, $\Delta J = 2$), is stronger when Dy³+ occupies low-symmetry sites, whereas the blue emission is enhanced in high-symmetry environments. The asymmetry ratio ($R = I_{ED}/I_{MD}$) serves as an important indicator of the local environment of Dy³+ ions. Calculated R values are 4.10439 (R = 1 mol), 4.3254 (R = 2 mol), 4.47451 (R = 4 mol), 3.90153 (R = 6 mol), 2.99877 (R = 8 mol), and 1.09075 (R = 10 mol). All R values greater than 1 indicate that Dy³+ ions occupy non-inversion-symmetric Y³+ sites.

Furthermore, as the Dy³⁺ doping concentration increases, the positions and shapes of all emission peaks remain essentially unchanged, indicating negligible spectral shift. At low concentrations (x = 1-4 mol%), the emission intensity increases with Dy³⁺ content. The optimal doping concentration is 4 mol%, beyond which the emission intensity decreases due

to concentration quenching (QC), as illustrated in Fig. 2b. This quenching arises from enhanced non-radiative (NR) energy transfer among Dy³⁺ ions, primarily via cross-relaxation processes such as ${}^4F_{9/2} + {}^6H_{15/2} \rightarrow [{}^6F_{7/2} + ({}^4F_{9/2}, {}^6H_{7/2})]$ and $[{}^6F_{3/2} + ({}^6F_{11/2}, {}^6H_{9/2})]$. Higher doping levels may also induce crystal defects, further reducing luminescence. Consequently, the NYG: 4 mol% Dy³⁺ sample was selected as the representative material for subsequent indepth analysis.

It is well known that concentration quenching can be attributed to the critical energy transfer between activator ions, which strongly depends on the distance between dopant ions.

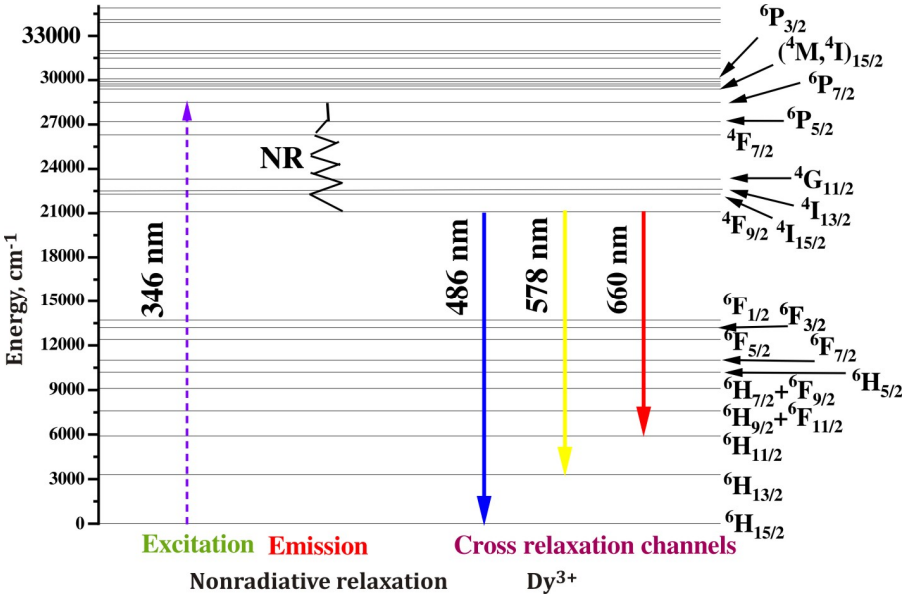


Fig. 3. Energy level diagram of Dy³⁺ ions.

3.3. Judd-Ofelt (J-O) analysis

The optical transition characteristics of trivalent rare-earth ions can be described by the Judd-Ofelt (J-O) theory, independently proposed by B. R. Judd and G. S. Ofelt in the early 1960s. Since its establishment, this theory has been widely applied, and a standard computational procedure has been developed. However, in most cases, this standard procedure is only suitable for rare-earth-doped transparent materials (such as crystals and glasses), as it requires absorption spectra as input data.

To overcome the limitation imposed by sample transparency, various modified J-O approaches have been developed in recent years to investigate the optical transition properties of rare-earth ions. In this study, we adopted the method proposed by Zhang et al.[19-21] to calculate the J-O parameters and explore the influence of dopant concentration on optical transitions. According to Zhang et al., the relative J-O parameters $\Omega'_{\lambda}(\lambda=2,4,6)$ can be determined by first obtaining the diffuse reflectance spectra of the samples and then converting them into relative absorption spectra using the Kubelka-Munk function as expressed in Eq. (4):

$$a'(v) = C \frac{[1 - R(v)]^2}{2R(v)},$$
 (4)

where R(v) represents the reflectance at wavenumber v; C is a constant related to the sample's morphology, particle size, and loading amount; and a'(v) denotes the relative absorbance. Fig. 4

presents the relative absorption spectra obtained for samples with different Dy³+ doping concentrations. It should be noted that the spectral intensities of all samples have been normalized to the strongest absorption peak corresponding to the $^6H_{15/2} \rightarrow ^6H_{9/2}/^6F_{11/2}$ transition.

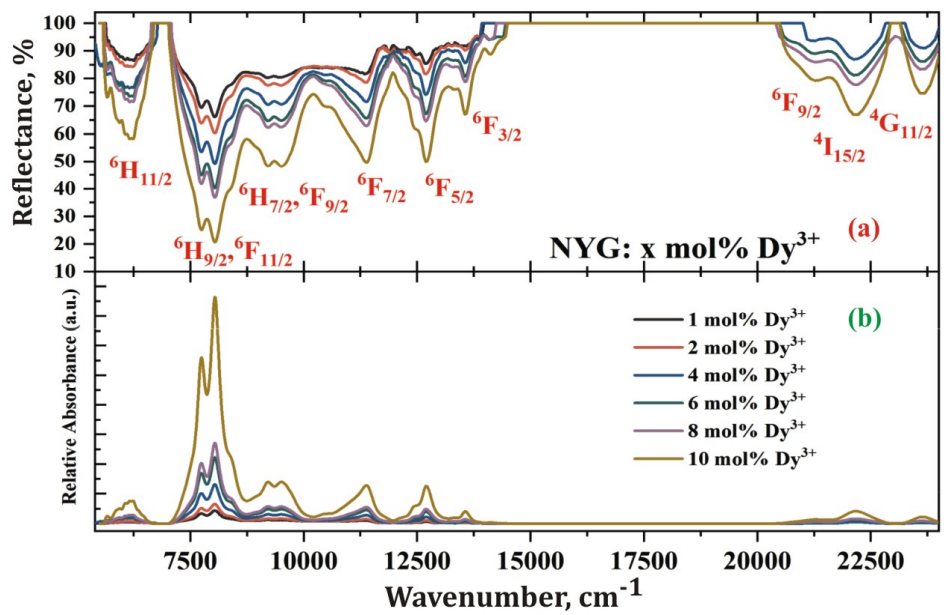


Fig. 4. Normalized relative absorption spectra of NYG: x Dy³⁺ phosphors.

From Fig. 4, nine distinct narrow absorption peaks can be clearly observed, corresponding to transitions from the ground state $^6\mathrm{H}_{15/2}$ to the excited states $^6\mathrm{H}_{11/2}$, $^6\mathrm{H}_{9/2}/^6\mathrm{F}_{11/2}$, $^6\mathrm{H}_{7/2}/^6\mathrm{F}_{9/2}$, $^6\mathrm{F}_{7/2}$, $^6\mathrm{F}_{5/2}$, $^6\mathrm{F}_{5/2}$, $^6\mathrm{F}_{9/2}$, $^4\mathrm{I}_{15/2}$, and $^4\mathrm{G}_{11/2}$. The normalized spectra indicate that the intensities of each transition vary with the Dy³+ doping concentration, suggesting that the dopant content influences the optical transition characteristics of the samples.

Once the relative absorption spectra are obtained, the next step in the J-O analysis is to calculate the relative experimental oscillator strengths $f'_{\rm exp}$. The relative experimental oscillator strength for a specific transition in the absorption spectrum can be determined using the following definition [22].

$$f_{\rm exp}^{\,\prime} = \frac{mc^2}{\pi e^2} \int a^{\,\prime}(v) dv \,, \tag{5}$$

where m and c represent the mass of the electron and the speed of light in vacuum, respectively. At the same time, π and e denote the mathematical constant π and the elementary charge of the electron. It should be noted that, unless otherwise specified, all physical quantities in this work are expressed in Gaussian units. According to the J-O theory, the theoretical oscillator strength for electric dipole-allowed f-f transitions of rare-earth ions (RE³+) can be expressed as follows[23]:

$$f_{th}^{ED} = \frac{8\pi^2 mcv}{3h(2J+1)} \frac{(n^2+2)^2}{9n} \sum_{\lambda=2,4,6} \Omega_{\lambda} (\langle \psi J | U^{\lambda} | \psi' J' \rangle)^2, \tag{6}$$

where n represents the refractive index of the studied host material; J and J' denote the angular momentum quantum numbers of the initial and final states involved in the f-f transitions, while $\langle \psi J | U^{\lambda} | \psi' J' \rangle$ and $\Omega_{\lambda}(\lambda=2,4,6)$ represent the reduced matrix elements and J-O parameters, respectively.

Let $f_{\rm exp}' = f_{th}^{\it ED}$, then each electric-dipole transition observed in Fig. 4 can be represented by one equation. By considering all allowed electric-dipole transitions, a set of equations containing three unknowns (i.e., the J-O parameters) can be established. These unknown J-O parameters can then be determined using the least-squares method. It should be emphasized that, since the relative experimental oscillator strength was used in Eq. (5), the J-O parameters obtained via least-squares fitting are relative values, denoted Ω_{λ} .

By substituting the relative J-O parameters Ω_{λ} into Eq. (6), the corresponding relative theoretical oscillator strengths $f_{i\text{-}th}^{\prime}$ can be obtained. The relative oscillator strengths derived from both experimental and theoretical calculations are summarized in the Table. 1. To evaluate the reliability of the J-O analysis, the absolute error of the relative oscillator strengths was calculated using the following equation, with the resulting errors also listed in the Table. 1[24].

$$\delta_{rms} = \sqrt{\frac{\sum_{i}^{N} (f'_{i-exp} - f'_{i-th})^{2}}{N - 3}},$$
(7)

where $f_{i-exp}^{'}$ and f_{i-th}^{ED} represent the relative experimental and theoretical oscillator strengths for the i-th transition, respectively, and N is the total number of transitions involved in the J-O calculation. A comparison of the results in the Table. 1 shows that the relative experimental oscillator strengths agree well with their corresponding relative theoretical values. Moreover, the absolute errors δ_{rms} for all samples are small and remain below most of the oscillator strength values. These findings indicate that the calculated results are highly reliable.

Table 1. Relative experimental oscillator strengths, relative theoretical oscillator strengths, and errors of Dy³⁺ in NYG: x mol% Dy³⁺ (x=1, 2, 4, 6, 8, 10) phosphors.

Transition	Relative experimental oscillator strengths, 10 ⁻⁸						
level	1 mol%	2 mol%	4 mol%	6 mol%	8 mol%	10 mol%	
$^{6}\mathrm{H}_{11/2}$	7.43	10.4	31.1	29.87	35.54	94.58	
$^{6}\mathrm{H}_{9/2}/^{6}\mathrm{F}_{11/2}$	64.44	111.92	186.69	287.21	297.64	670.16	
$^{6}F_{9/2}/^{6}H_{7/2}$	36.17	42.89	64.86	104.82	124.22	281.95	
$^{6}F_{7/2}$	9.21	14.22	25.32	45.15	52.03	109.91	
$^{6}F_{5/2}$	2.76	5.93	12.19	22.88	28.23	73.38	
$^{6}F_{3/2}$	1.87	1.52	2.86	5.66	7.51	20.15	
$^{4}F_{9/2}$	7.43	10.4	1.4	4.71	11.59	26.92	
$^{4}I_{15/2}$	64.44	111.92	6.71	16.31	23.81	59.54	
δ_{rms}	2.28	1.71	14.65	12.51	20.69	60.68	
$^{6}\mathrm{H}_{11/2}$	5.56	9.75	24.88	30.14	34.12	84.49	
$^{6}\mathrm{H}_{9/2}/^{6}\mathrm{F}_{11/2}$	64.68	112.01	187.48	287.19	297.86	671.54	
$^{6}F_{9/2}/^{6}H_{7/2}$	35.07	42.24	61.62	103.86	122.09	272.84	
$^{6}F_{7/2}$	13.62	17.06	37.81	50.02	61.76	149.06	
$^{6}F_{5/2}$	2.65	3.68	14.67	14.79	19.52	51.81	
$^{6}F_{3/2}$	0.5	0.69	2.76	2.79	3.68	9.77	
$^{4}F_{9/2}$	5.56	9.75	2.77	3.57	4.45	10.84	
$^{4}I_{15/2}$	64.68	112.01	7.66	8.78	10.2	25.91	

To further elucidate the effect of Dy $^{3+}$ concentration on the optical transition properties, it is necessary to determine the absolute values of the J-O parameters. According to the J-O parameter calculation method proposed by Zhang et al., the absolute values can be obtained through the following calibration procedure. In this calibration process, the radiative lifetime of the Dy $^{3+}$ $^4F_{9/2}$ level is selected as a reference scalar to calibrate the J-O parameters. By substituting the relative J-O parameters into the following formula, the relative electric-dipole transition probabilities from the $^4F_{9/2}$ level to its lower-lying levels l' can be determined.

$$A_{^{4}F_{9/2} \to I'}^{ED} = \frac{64\pi \,^{4}e^{2}v_{i}^{3}n(n^{2}+2)^{2}}{27h(2J+1)} \sum_{\lambda=2,4,6} \Omega'_{\lambda} \left(\left\langle \psi J \middle| U^{\lambda} \middle| \psi' J' \right\rangle \right)^{2}. \tag{8}$$

Subsequently, the total relative electric-dipole transition probability of the ${}^4F_{9/2}$ level can be calculated using the following equation:

$$A_{{}^{4}F_{9/2}}^{'ED} = \sum_{I'} A_{{}^{4}F_{9/2} \to I'}^{'ED} = \sum_{I'} \frac{64\pi^{4}e^{2}v_{I}^{3}n(n^{2} + 2)^{2}}{27h(2J + 1)} \sum_{\lambda = 2,4,6} \Omega'_{\lambda} \left(\left\langle \psi J \middle| U^{\lambda} \middle| \psi' J' \right\rangle \right)^{2}. \tag{9}$$

If the transition from level l to its lower levels l' also satisfies the selection rules for magnetic dipole (MD) transitions, the corresponding MD transition probability can be calculated using the following equation:

$$A_{i \to l'}^{MD} = \frac{16\pi^4 e^2 n^3}{3h(2J+1)m^2 c^2} \left| \left\langle (S,L)J | L + 2S | (S',L')J' \right\rangle \right|^2. \tag{10}$$

In Eqs. (9) and (10), J = 9/2. The squared reduced matrix elements $|\langle (S,L)J|L + 2S|(S',L')J'\rangle|$ for the magnetic dipole (MD) transitions are available in the literature. For clarity, the MD transition probabilities of Dy³⁺ are also listed in the Table. 2. The physical meanings of the other symbols remain the same as previously described. In this work, the absolute probabilities of Dy³⁺ MD transitions in the NYG host were calculated and are presented in a Table. 2 [25].

Table 2. Values of $A_{l\to l'}^{MD}$ for Dy³⁺ in NCZLB glasses (taken from Ref. [25]) and NYG phosphors.

Transition level (${}^{4}F_{9/2} \rightarrow$)	$A_{l\to l'}^{MD}$ NCZLB: Dy ³⁺ (n = 1.58)	$A_{l\to l'}^{MD}$ NYG: Dy ³⁺ (n = 1.825)		
⁶ F _{1/2}	0	0.00		
$^{6}F_{3/2}$	0	0.00		
⁶ F _{5/2}	0	0.00		
⁶ F _{7/2}	5.48	8.44		
$^{6}{ m H}_{5/2}$	0	0.00		
$^{6}\mathrm{H}_{7/2}$	2.65	4.08		
$^{6}F_{9/2}$	5.77	8.89		
$^{6}F_{11/2}$	51.11	78.76		
$^{6}\mathrm{H}_{9/2}$	3.07	4.73		
$^{6}\mathrm{H}_{11/2}$	11.73	18.08		
$^{6}\mathrm{H}_{13/2}$	0	0.00		
⁶ H _{15/2}	0	0.00		
Total	79.81	122.99		

To calibrate the J-O parameters from relative to absolute values, the total absolute ED transition probability $A_{4F9/2}^{ED}$ of the ${}^{4}F_{9/2}$ level must be known. This value can be calculated using the following equation:

$$A_{4F9/2}^{\rm ED} = \frac{l}{\tau_{4F9/2}} - A_{4F9/2}^{\rm MD} , \qquad (11)$$

where, $A_{4F9/2}^{ED}$ represents the total MD allowed transition probability of the ${}^4F_{9/2}$ level, which is the sum of the individual MD transition probabilities listed in Table 2. The radiative lifetime of the ${}^4F_{9/2}$ level, $\tau_{4F9/2}$, can be determined from the fluorescence decay curve.

By substituting the values τ_r obtained from fitting, the total absolute electric-dipole transition probability of the $^4\mathrm{F}_{9/2}$ level can be calculated. Then, the absolute J-O parameters can be determined using the following equation

$$\Omega_{\lambda} = \frac{A_{4F_{0/2}}^{ED}}{A_{4F_{0/2}}^{ED}} \Omega'_{\lambda} . \tag{12}$$

Table 3. Judd-Ofelt parameters of Dy³⁺ in NYG doped with various concentrations.

Dy ³⁺ /mol%	1	2	4	6	8	10
$\Omega_2(10^{-20} { m cm}^2)$	6.61	9.59	3.96	0.96	8.71	8.71
$\Omega_4(10^{-20}\mathrm{cm}^2)$	11.61	7.43	4.17	5.96	6.39	5.64
$\Omega_6(10^{-20}\mathrm{cm}^2)$	1.25	0.95	4.24	1.38	1.72	1.95

The calculated absolute J-O parameters are listed in the Table. 3. After determining the absolute J-O parameters, the radiative transition characteristics of NYG: Dy³+ phosphors at different Dy³+ concentrations can be further evaluated. The radiative transition probabilities, branching ratios, and lifetimes of the ${}^4F_{9/2}$ level to its lower-lying levels were calculated, and the results are presented in the Table. 4. It should be noted that the electric-dipole allowed transition probabilities were calculated using Eq. (11), while the magnetic-dipole allowed transition probabilities were calculated using Eq. (10). The fluorescence branching ratio $\beta_{4F9/2 \rightarrow l}$ for the ${}^4F_{9/2} \rightarrow l$ transition can be expressed as follows:

$$\beta_{4F9/2 \to l} = \frac{A_{4F9/2 \to l}}{\sum_{l} A_{4F9/2 \to l}} , \qquad (13)$$

where $A_{4F9/2\rightarrow l}$ represents the radiative transition probability from the ${}^4F_{9/2}$ level to the lower-lying level l. As shown in the Table. 4: (1) the calculated radiative lifetimes of the ${}^4F_{9/2}$ level for Dy³⁺ at different doping concentrations are in good agreement with the experimental data, indicating the high reliability of the J-O calculations; (2) the radiative lifetimes of the ${}^4F_{9/2}$ level are similar across all samples, further confirming that the radiative lifetime of Dy³⁺ in the NYG matrix is nearly independent of doping concentration, which is highly consistent with the fitting results; (3) moreover, the transitions from ${}^4F_{9/2}$ to the ${}^6H_{13/2}$ and ${}^6H_{15/2}$ levels exhibit large fluorescence branching ratios, which is an intrinsic characteristic of Dy³⁺ ions.

Table 4. Radiative transition rates A^{ED} and A^{MD} , fluorescence branching ratios β , and radiative transition lifetimes τ of Dy³⁺ in NYG:x mol% Dy³⁺ (x = 1, 2, 4, 6, 8, 10)

radiative transition lifetimes τ of Dy ³⁺ in NYG:x mol% Dy ³⁺ (x = 1, 2, 4, 6, 8, 10)							
Initial level	Final level	$A^{ED}/(A^{MD})$, s^{-1}	β, %	τ, ms	$A^{ED}/(A^{MD})$, s^{-1}	β, %	τ, ms
1	2	3	4 5		6 7		8
			mol%Dy	3+	NYG:2 mol%Dy ³⁺		
4-	$^{6}F_{1/2}$	0/	0.00	0.44995	0/	0.00	0.41761
	⁶ F _{3/2}	0/	0.00		0/	0.00	
	$^{6}F_{5/2}$	7.58/	0.63		18.35/	0.83	
	$^{6}F_{7/2}$	15.32/11.45	1.69		23.50/8.44	1.44	
	H _{5/2}	9.67/	1.02		14.79/	0.67	
	⁶ H _{7/2}	42.80/5.54	3.59		52.42/4.08	2.54	
$^{4}F_{9/2}$	$^{6}F_{9/2}$	18.40/12.06	2.67		34.99/8.89	1.97	
	⁶ F _{11/2}	33.17/106.80	6.29		56.51/78.76	6.09	
	H _{9/2}	29.53/6.42	2.28		41.20/4.73	2.07	
	⁶ H _{11/2}	79.61/24.51	6.59		156.73/18.08	7.87	
	⁶ H _{13/2}	1031.61/	59.52		1460.52/	65.72	
	⁶ H _{15/2}	511.93/	15.72		240.45/	10.82	
15/2		NYG:4 mol%Dy³+			NYG:6 mol%Dy³+		
	6F _{1/2}	0/	0	0.30883	0/	0	0.21555
	$^{6}F_{3/2}$	0/	0		0/	0	
	6F _{5/2}	18.00/	0.81		18.11/	0.82	
	6F _{7/2}	18.27/8.44	1.2 0.39		21.28/8.44	1.34 0.55	
	H _{5/2} 6H _{7/2}	8.63/ 37.08/4.08	1.85		12.20/ 46.08/4.08	2.26	
$^{4}F_{9/2}$	6F _{9/2}	21.28/8.89	1.36		29.21/8.89	1.71	
	6F _{11/2}	48.19/78.76	5.71		52.90/78.76	5.92	
	H _{9/2}	36.28/4.73	1.85		39.16/4.73	1.97	
	⁶ H _{11/2}	154.81/18.08	7.78		155.24/18.08	7.8	
	$^{6}H_{13/2}$	1470.40/	66.16		1461.86/	65.78	
	$^{6}H_{15/2}$	286.53/	12.89		263.44/	11.85	
		NYG:8 mol%Dy³+		NYG:10 mol%Dy ³⁺			
	⁶ F _{1/2}	0/	0.00	0.20313	0/	0.00	0.14795
	$^{6}F_{3/2}$	0/	0.00		0/	0.00	
	$^{6}F_{5/2}$	16.73/	0.75		16.58/	0.47	
	$^{6}F_{7/2}$	21.72/8.44	1.36		20.66/8.44	1.12	
⁴ F _{9/2}	$H_{5/2}$	13.24/	0.60		11.98/	0.40	
	$^{6}H_{7/2}$	49.61/4.08	2.42		46.53/4.08	2.11	
	$^{6}F_{9/2}$	30.57/8.89	1.78		27.69/8.89	1.17	
	$^{6}F_{11/2}$	52.24/78.76	5.89		50.41/78.76	5.37	
	H _{9/2}	39.36/4.73	1.98		38.32/4.73	1.72	
	⁶ H _{11/2}	145.89/18.08	7.38		144.90/18.08	5.51	
	⁶ H _{13/2}	1421.06/	63.94		1420.77/	56.77	
	⁶ H _{15/2}	309.05/	13.91		321.66/	25.36	
	13/2		1	I	· · · · · · · · · · · · · · · · · · ·	l .	

3.5. Concentration dependence of internal quantum efficiency

The internal quantum efficiency (IQE) is a crucial parameter for evaluating the performance of rare-earth-doped luminescent materials. In this section, the effect of Dy³+ doping concentration on the emission IQE of the $^4F_{9/2}$ level is discussed. The *IQE* is defined as the ratio of the measured fluorescence lifetime $\bar{\tau}$ to the radiative lifetime $\tau_{4F9/2}$ of the $^4F_{9/2}$ level, and can be expressed as:

$$\eta = \frac{\overline{\tau}}{\tau_{4F9/2}},\tag{14}$$

where the radiative lifetime $\tau_{4F9/2}$ has been determined from the fluorescence decay curves and is presented in Fig. 5a. The fluorescence lifetime $\bar{\tau}$ can be calculated using the following expression:

$$\overline{\tau} = \frac{\int_0^\infty I(t)tdt}{\int_0^\infty I(t)dt},\tag{15}$$

where I(t) represents the emission intensity at time t, i.e., the fluorescence decay. The fluorescence lifetimes calculated using Eq. (15) are: $\bar{\tau}$ (x=1 mol%)=0.44995 ms, $\bar{\tau}$ (x=2 mol%)=0.41761 ms, $\bar{\tau}$ (x=4 mol%)=0.30883 ms, $\bar{\tau}$ (x=6 mol%)=0.21555 ms, $\bar{\tau}$ (x=8 mol%)=0.20313 ms, and $\bar{\tau}$ (x=10 mol%)=0.14795 ms. As shown in Fig. 5b, these results clearly reveal a concentration-dependent trend: with increasing Dy³+ doping concentration, the lifetime decreases gradually due to non-radiative (NR) transitions. The sufficiently short lifetimes further indicate that NYG: Dy³+ phosphors possess promising potential for w-LED applications.

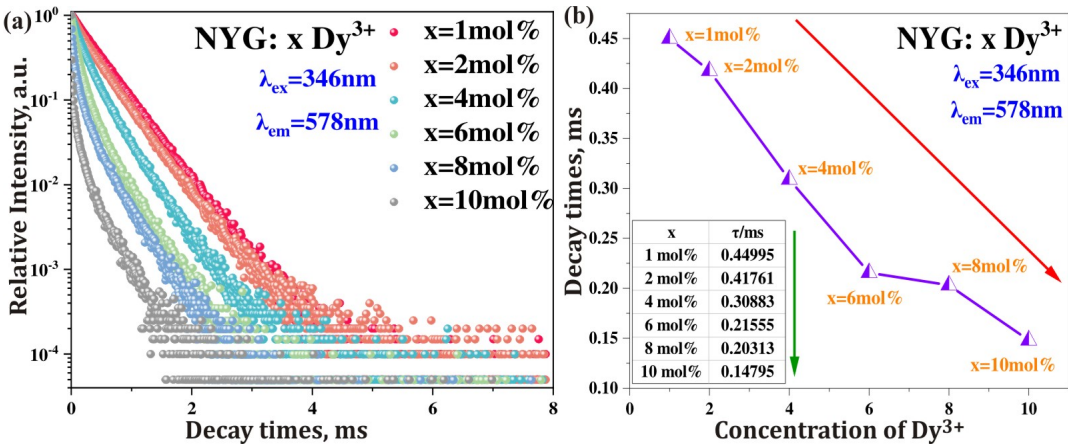


Fig. 5. (a) Fluorescence decay curves of NYG: x mol% Dy³⁺ samples; (b) Plot of fluorescence lifetimes of NYG: $x \text{ Dy}^{3+}$ samples as a function of Dy³⁺ doping concentration.

Table 4 lists the fluorescence lifetimes $\bar{\tau}$, the radiative lifetimes $\tau_{4F9/2}$ of the $^4F_{9/2}$ level, and the internal quantum efficiencies (η) of NYG samples with different Dy³+ concentrations. Using Eq. (14), the internal quantum efficiencies of NYG: x Dy³+ samples were calculated as follows: $\eta(x=1 \text{ mol}\%)=102.64\%$, $\eta(x=2 \text{ mol}\%)=104.10\%$, $\eta(x=4 \text{ mol}\%)=80.35\%$, $\eta(x=6 \text{ mol}\%)=65.34\%$, $\eta(x=8 \text{ mol}\%)=57.99\%$, and $\eta(x=10 \text{ mol}\%)=39.16\%$. The internal quantum efficiency generally decreases as the Dy³+ concentration in NYG increases.

4. Conclusions

A series of Dy³⁺-doped NYG phosphors (x = 1-10 mol%) were successfully synthesized via a high-temperature solid-state reaction. X-ray diffraction (XRD) analysis confirmed that all samples retained the crystal structure of the NYG host, indicating that the incorporation of Dy3+ did not disrupt the lattice framework. This host not only provides suitable lattice sites for Dy³⁺ ions but also possesses a wide bandgap of 5.493-5.864 eV, offering an appropriate energy environment for efficient photoluminescence. Under 346 nm excitation, the samples exhibited characteristic Dy³⁺ emission bands in the blue (486 nm), yellow (578 nm), and red (660 nm) regions, corresponding to the ${}^4F_{9/2} \rightarrow {}^6H_{15/2}$, ${}^4F_{9/2} \rightarrow {}^6H_{13/2}$, and ${}^4F_{9/2} \rightarrow {}^6H_{11/2}$ transitions, respectively. The emission intensity reached its maximum at a Dy3+ doping concentration of 4 mol%. Moreover, to elucidate the influence of Dy³+ doping on the optical transition properties of NYG, the J-O theory was systematically applied to samples with different Dy3+ concentrations. The J-O intensity parameters were derived from diffuse reflectance spectra, and their variation trends were analyzed. The results show that as Dy3+ concentration increases, the internal quantum efficiency of NYG: Dy3+ phosphors generally decreases. These findings provide important theoretical insights into the energy transfer dynamics and structure-property relationships in rare-earth-doped germanate phosphors.

Funding and acknowledgment. This work is supported by the National Natural Science Foundation of Liaoning Province, China (approval number: 2025-MS-310), Liaoning Province Science and Technology Plan Joint Program (Natural Science Foundation-Doctoral Research Start-up Project) (approval number: 2024-BSLH-137), and National Natural Science Foundation of China (approval number: 52201065).

Conflict no interest. The authors declare that they have no known competing financial interests or personal relationships that could have influenced the work reported in this paper.

Data availability. The data that support the findings of this study are available from the corresponding author upon reasonable request.

References

- He, E., Chen, X., Wu, Y., Cui, Y., Wang, T., Li, F., Han, Q., Zuo, X., & Liu, N. (2025). Efficient deep-red-emitting CaMg₂La₂W₂O₁₂: Mn⁴⁺, Nd³⁺ phosphor toward indoor plant cultivation LED lighting. *Journal of Luminescence*, 121578.
- Mao, Y., Zhao, X., Shi, S., & Fu, L. (2025). Structure and optical properties of Mn⁴⁺-doped Li₆CaLa₂Ta₂O₁₂ phosphor for temperature sensing and latent fingerprint detection. *Journal of Molecular Structure*, 143345.
- 3. Peng, C., Tang, B., Wei, M., Zhang, X., Molokeev, M. S., Zhang, H., & Lei, B. (2025). Constructing Efficient and Thermally-stable Far Red Emitting Phosphor with Excellent Response to Phytochrome Pfr for Indoor Agriculture. *Journal of Alloys and Compounds*, 183960.
- Sonkusare, K., Tikale, R., Taikar, D. R., & Dhoble, S. J. (2025). Color tunable luminescence and energy transfer behavior of Dy³⁺, Eu³⁺ co-doped Na₂MgPO₄F phosphor for light emitting devices. *Journal of Molecular Structure*, 144122.
- 5. Yuan, C., Peng, X., Li, R., Zhang, Y., Deng, C., & Cui, R. (2025). A novel thermally-stable red phosphor Ba₆La₂Ga₄O₁₅: Eu³⁺ for WLEDs, anti-counterfeit inks, and fingerprint analysis. *Journal of Photochemistry and Photobiology A: Chemistry*, 116804
- 6. Niu, Y., Wu, F., Zhuo, Y., Li, J., Zhang, Q., Teng, Y., Xie, X., Dong, H. & Mu, Z. (2025). Photochromic and long persistent luminescence properties of Bi³⁺ doped SrGa₄O₇. *Journal of Photochemistry and Photobiology A: Chemistry*, 116800.
- Wang, Y., Li, Z., Xue, M., Lai, Z., & Cao, W. (2026). Recent progress in Eu²⁺ activated red phosphors for white LEDs and laser displays: focusing on efficient host screening and innovative structural design. *Coordination Chemistry Reviews*, 546, 217060.
- 8. Liu, F., Zhao, J., Tu, R., Fu, Y., Wang, Y., Lu, J., & Leng, Z. (2025). Energy Transfer Engineering in Matrix-Sensitized NaBa₁₀Y₅W₄O₃₀: Sm³⁺ Orange-Red Phosphors for Solid-State Lighting. *Journal of Solid State Chemistry*, 125681.
- Yang, R., Song, K., Zheng, Y., Zhan, C., Wang, Y., Lin, C., Zhou, T., Zhuang, Y. & Xie, R. J. (2025). Wide-Range Tuning of Trap Depths in Double Perovskite Phosphors Enabling Tunable NIR Persistent Luminescence. Advanced Powder Materials, 100343.

- 10. Du, Y., Jabeen, S., Zhao, H., Zhang, Y., Yang, Y., Yang, Y., Xie, M., Yu, R. & Yu, R. (2025). Oleic acid passivation engineering enables humidity-stable SrLaZnO₃₋₅: Sm³⁺ red phosphors for high-performance white LEDs and fingerprint visualization with level III details. *Applied Materials Today*, *47*, 102931.
- Zhang, J., Liu, B., Dai, Y., & Han, B. (2020). Synthesis and luminescence properties of novel host-sensitized germanate phosphors NaYGeO₄: Ln (Ln= Eu³⁺, Sm³⁺, Dy³⁺). Optik, 203, 163944.
- Wang, E., Feng, K., Li, J., Zhou, X., & Sun, X. (2022). Luminescence characteristics of NaYGeO₄: Bi³⁺/Tb³⁺/Eu³⁺ phosphors. *Journal of Luminescence*, 250, 119108.
- 13. Zhao, W., Feng, X., & Fan, B. (2020). Novel color tunable phosphors NaYGeO₄: Tm³⁺, Tb³⁺, Eu³⁺ for ultraviolet excited white LEDs with good thermal stability. *Journal of Materials Science: Materials in Electronics*, *31*(17), 14434-14442.
- 14. Ansari, E., Patle, S. K., Ugemuge, N. S., Kadam, A. R., & Dhoble, S. J. (2025). Structural and spectroscopic analysis of GdSr₃(PO₄)₃: Dy³⁺ phosphors for white LED applications. *Journal of Molecular Structure*, 143856.
- 15. Wang, N., Li, Y., Yang, L., Zhang, Y., Guo, H., Cui, R., Zhang, J. & Deng, C. (2025). Achieving spectrally tunable properties in Ca₉ZnLi(PO₄)₇ by utilizing energy transfer between Eu²⁺ and Dy³⁺ ions. *Journal of Alloys and Compounds*, 183449.
- Kang, S. H., Kim, S. J. (2025). Enhanced photocatalytic reaction of (TiO₂–WO₃) on Sr₄Al₁₄O₂₅:Eu,Dy long-lasting phosphor. J. Mater. Sci.: Mater. Electron. 36(26), 1726–1737.
- 17. Zhuang, P., Liu, W., Cao, H., Lin, Y., Guo, Y., Zhang, J., & Zhang, Y. (2025). Tunable warm white emission in Eu³⁺/Dy³⁺ codoped K₂Y(WO₄)(PO₄) phosphors for solid-state lighting. *Ceramics International*.
- Xia, Z., Li, R., Liu, F., Zhou, W., Zhao, W., Meng, W., Song, M. & Xue, J. (2025). Dual-luminescent Sc₂(MoO₄)₃: Dy³⁺/Eu³⁺ phosphor system: energy transfer dynamics and high-sensitivity temperature sensing. RSC advances, 15(35), 28994-29002
- 19. Zhang, Y., Chen, B., Xu, S., Li, X., Zhang, J., Sun, J., Zhang, X., Xia, H. & Hua, R. (2019). Reply to the 'Comment on "A universal approach for calculating the Judd–Ofelt parameters of RE³⁺ in powdered phosphors and its application for the β-NaYF₄: Er³⁺/Yb³⁺ phosphor derived from auto-combustion-assisted fluoridation" by D. Zhang, Q. Xu and Y. Zhang, Phys. Chem. Chem. Phys., 2019, 21. Physical Chemistry Chemical Physics, 21(20), 10840-10845.
- Tang, H., Qin, Y., Zhao, X., Liu, L., Huang, Z., Quan, J., Tang, Y. & Zhu, J. (2024). Highly thermostable and color tunable Dy³⁺/Sm³⁺ co-doped germanate phosphors for solid-state lighting. *Journal of Alloys and Compounds*, 1005, 176237.
- Jose, J. R., Jose, T. A., Ashok, A. J., Joseph, C., & Biju, P. R. (2024). Cool white light emitting Dy³⁺ activated KNaCa₂(PO₄)₂ phosphor for outdoor lighting and optical thermometric applications. *Journal of Alloys and Compounds*, 1006, 176304.
- 22. Hua, Y., Ran, W., & Yu, J. S. (2021). Excellent photoluminescence and cathodoluminescence properties in Eu³⁺ activated Sr₂LaNbO₆ materials for multifunctional applications. *Chemical Engineering Journal*, 406, 127154.
- 23. Tamilmani, V., Mondal, M., Rai, V. K., & Mishra, A. K. (2021). Tunable luminescence from yttrium oxide flowers using asparagine as shape modifier. *Journal of Alloys and Compounds*, 857, 157575.
- Kaewnuam, E., Chanthima, N., Jayasankar, C. K., Kim, H. J., & Kaewkhao, J. (2016). Optical, luminescence and judd-oflet study of Eu3+ doped lithium yttrium borate glasses for using as laser gain medium. Key Engineering Materials, 675, 364-367.
- Verma, R. S., Gupta, R., & Joshi, G. K. (2002). Calculation of Judd-Ofelt intensity parameters. *Journal of the Indian Chemical Society*, 79(10), 802-806.

Liu, S., Gao, D., Dong, J., Yin, H., Liu, H., Wang, L., Song, W. (2026). Judd-Ofelt Analysis and Concentration-Dependent Luminescence Quenching Behavior of Dy³⁺-Doped NaYGeO₄ Phosphors Prepared by Solid-State Reaction. *Ukrainian Journal of Physical Optics*, *27*(1), 01040 – 01053. doi: 10.3116/16091833/Ukr.J.Phys.Opt.2026.01040

Анотація. У цьому дослідженні серію люмінофорів NaYGeO₄ (NYG): Dy³⁺ з різною концентрацією легувальної домішки Dy³⁺ було успішно синтезовано за допомогою звичайного методу високотемпературної твердофазної реакції. Рентгенівський дифракційний аналіз підтвердив, що всі зразки демонстрували чисту фазу NYG без виявлених вторинних фаз. Для систематичного дослідження поведінки концентраційного гасіння та термічної стабільності люмінесценції було всебічно схарактеризувано властивості фотолюмінесценції зразків. Крім того, для глибшого розуміння характеристик оптичних переходів іонів Dy³⁺ були використані спектри дифузного відбиття, вимірювання флуоресцентного спаду та теорію Джадда-Офельта. Результати показують, що внутрішня квантова ефективність рівня Dy³⁺ 4F_{9/2} поступово зменшується зі збільшенням концентрації легувальної домішки.

Ключові слова: люмінесценція, теорія Джадда-Офельта, NaYGeO₄, люмінофори